Mesoscale Momentum Budget in a Midlatitude Squall Line: A Numerical Case Study

KUN GAO,* DA-LIN ZHANG,** MITCHELL W. MONCRIEFF AND HAN-RU CHO**

National Center for Atmospheric Research,† Boulder, Colorado

(Manuscript received 20 April 1989, in final form 9 November 1989)

ABSTRACT

A mesoβ-scale momentum budget and its effect on larger-scale mean flow in a midlatitude mesoscale convective system are investigated using a numerical simulation of an intense squall line that occurred during 10–11 June 1985 PRE-STORM. It is found that the momentum generation normal to the line associated with the latent heating and cooling contributes most significantly to the momentum budget and determines the mesoβ-scale internal structure and evolution of the squall line. The momentum generation along the line contributes to the initial development of a mesovortex but has little effect on the final vertical structure of the along-line flow. Both vertical and horizontal momentum advection have significant contributions, particularly to the vertical mixing of the along-line flow; and this component of the horizontal momentum is locally transported downgradient. It is also found that for midlatitude convective systems, convectively generated downdrafts can play as prominent a role as updrafts in vertically transporting horizontal momentum within both convective and stratiform regions.

The momentum flux associated with the mesoβ-scale circulations of the simulated squall line is found to agree with previous observational investigations, namely, normal to the line the squall system transports horizontal momentum in a countergradient sense while parallel to the line the transport is downgradient. Implications with respect to the convective momentum parameterization are discussed in the context of the mesoβ-scale momentum budget.

1. Introduction

There has been considerable interest during the last few decades in the effects of momentum transports by cumulus convection on modifying the meso- and larger-scale circulation systems (e.g., Palmen and Newton 1969; Schneider and Lindzen 1976; Cho 1985). Various diagnostic computations for tropical weather systems have clearly revealed the existence of large apparent momentum sources in the budget equations that can be attributed to subgrid-scale convective processes (e.g., Stevens 1979; LeMone 1983; LeMone et al. 1984). There have also been suggestions that some distinct features in the large-scale flow are caused by cumulus momentum transport, such as the development of anticyclonic wind perturbations in the upper troposphere associated with mesoscale convective systems (MCSs) (Ninomiya 1971; Fritsch and Maddox 1981; Maddox et al. 1981). Furthermore, downward convective transport of horizontal momentum has been suggested as one of the mechanisms whereby the ageostrophic low-level jet along the Mei-Yu front over eastern Asia may be generated (Matsumoto 1972; Ninomiya and Akiyama 1974). Moncrieff (1985) provided a review of previous studies related to this subject.

Nevertheless, there is still no consensus on the importance of convective momentum transports in determining the structure, evolution and organization of MCSs. For example, the parameterization of vertical transport of horizontal momentum due to subgrid-scale processes has yet to be properly considered in almost all of the existing mesoscale numerical prediction models (e.g., Anthes et al. 1987; Phillips 1979; Chang et al. 1981; Kaplan et al. 1982), but considerable successes achieved with those models in predicting MCSs have been reported in the literature. This indicates that the subgrid-scale momentum transports by cumulus clouds may not be as crucial as heat and moisture in convective parameterization. In fact, little is known regarding to the sensitivity of numerical models to the parameterized transport of horizontal momentum. Zhang and Fritsch (1988) noted that a simulation of the 1977 Johnstown MCSs is insensitive to the momentum flux in the Fritsch and Chappell (1980) convective parameterization scheme in which the in-cloud horizontal momentum is treated as a conservative quantity.

Improvements in our understanding of convective momentum transports are primarily limited by: (i)

* On leave from Department of Geography, Hang-zhou University, People's Republic of China.

** Department of Physics, University of Toronto, Toronto, Ontario, Canada M5S 1A7.

† The National Center for Atmospheric Research (NCAR) is funded by the National Science Foundation.

Corresponding author address: Dr. Da-Lin Zhang, Department of Meteorology, McGill University, 850 Sherbrooke St. W, Montreal Quebec, Canada H3A 2K6.

horizontal pressure gradients and their variability on the convective or even mesoα-scale (Orlanski 1975) are difficult to evaluate, particularly in the tropics, and (ii) the diagnostic results of momentum transports cannot be independently and consistently verified against other meteorological observations. Recently, Flatau and Stevens (1987) estimated the momentum budget on a 30 km grid scale using the modified Fritsch–Chappell convective scheme and found that the impact of horizontal pressure gradients in a tropical squall line can have a magnitude comparable with other terms in the momentum equation. Although comprehensive momentum budgets associated with midlatitude MCSs have yet to be presented in the literature, the effect of the horizontal pressure gradient in midlatitude MCSs is believed to be more significant than that in tropical MCSs. The limitations in the use of real data for the momentum budget calculations have made numerical models a useful tool for investigating the convective transport properties. In this regard, Soong and Tao (1984) studied the vertical momentum transport of a tropical rainband using a two-dimensional cloud ensemble model with idealized initial conditions, and found that the results qualitatively support the aforementioned observational studies.

The purposes of this study are to: (i) examine the relative importance of various processes in the momentum budget equations in determining the mesoβ-scale flow structure and evolution of a MCS, and (ii) investigate the integral momentum transport effects of the MCS on the larger-scale mean flow, using a real-data numerical simulation of an intense squall line that occurred during 10–11 June 1985 Preliminary Regional Experiment for STORM[1] Central (PRE-STORM; Cunning 1986). In particular, Zhang et al. (1989) and Zhang and Gao (1989) (hereafter referred to as ZGP and ZG, respectively) showed that, with the conventional-network data as initial conditions, the PSU/NCAR (Pennsylvania State University/National Center for Atmospheric Research) three-dimensional, mesoscale hydrostatic model simulated remarkably well many of the mesoβ-scale structure and evolution of the squall line, as compared to available observations (e.g., Augustine and Zipser 1987; Johnson and Hamilton 1988; Rutledge et al. 1988). Specifically, the model reproduced the initiation of the squall line at nearly the correct time and location; the generation of a pre-squall mesolow, a squall-induced mesohigh and a wake low; the relative flow configuration of front-to-rear (FTR) motion at both upper and lower levels with an intermediate rear-to-front (RTF) flow; the maintenance and intensification of a mesovortex; and the leading convective rainfall followed by a transition zone and trailing stratiform precipitation (see cited papers for more details). Thus, confidence has been established that this particular simulation can be utilized to compute the momentum budget for the much-needed understanding of convective transport properties and momentum parameterization problems. In section 2, the basic methodology used for this study and the simulation results are briefly described. Sections 3 and 4 present the mesoβ-scale momentum budgets normal and parallel to the line, respectively, whereas section 5 describes the integral effects of the squall line on the larger-scale mean flow. The implication of the budget results with respect to the convective momentum parameterization is discussed in the final section.

2. Description of the simulation and methodology

The PSU/NCAR model used for the present study incorporates the Fritsch–Chappell (1980) cumulus parameterization scheme for the fine-mesh portion of the nested-grid model, and explicit calculations of cloud water (ice) and rainwater (snow) as predictive variables for both meshes (see Anthes et al. 1987; Zhang et al. 1988; Zhang 1989). Zhang and Gao showed that those model physics, particularly, the parameterized moist downdrafts, resolvable-scale water loading, evaporative cooling and melting, are essential in realistically reproducing the structure and evolution of the rear inflow jet, surface pressure perturbations and other mesoβ-scale features of the squall line. The model was initialized at 1200 UTC 10 June 1985 and integrated for 24 h with a fine-mesh length of 25 km (see ZGP for more details). Here one should note that the use of this grid size tends to produce aliasing of features on smaller scales, especially those along the leading line of the squall system. Nevertheless, we believe that the simulation produced a dynamically consistent four-dimensional high-resolution dataset with which the mesoscale momentum budget can be more meaningfully obtained than is possible with observational data (e.g., the PRE-STORM-network dataset). Furthermore, the general agreement between the simulation and observations is deemed adequate for using the model output to investigate the processes that lead to the successful simulation of the mesoβ-scale circulations.

Although a detailed description of the model simulation can be found in ZGP and ZG, Figs. 1 and 2 show a portion of the evolution of surface features and the vertical cross sections of horizontal relative flow, circulation vectors and deviation height fields from 12, 15 and 18 h simulations for convenience in later discussion. (Note that convective activity commenced at about 9 h into the simulation.) These three periods are chosen since they represent the system development at roughly three different stages: incipient, mature and dissipation. The most relevant features at the surface are the generation of a pre-squall mesolow, a squall-induced mesohigh and a wake low, and their positions relative to the leading convective line. Vertical cross sections through these surface pressure perturbations

[1] STORM: STormscale Operational and Research Meteorology.

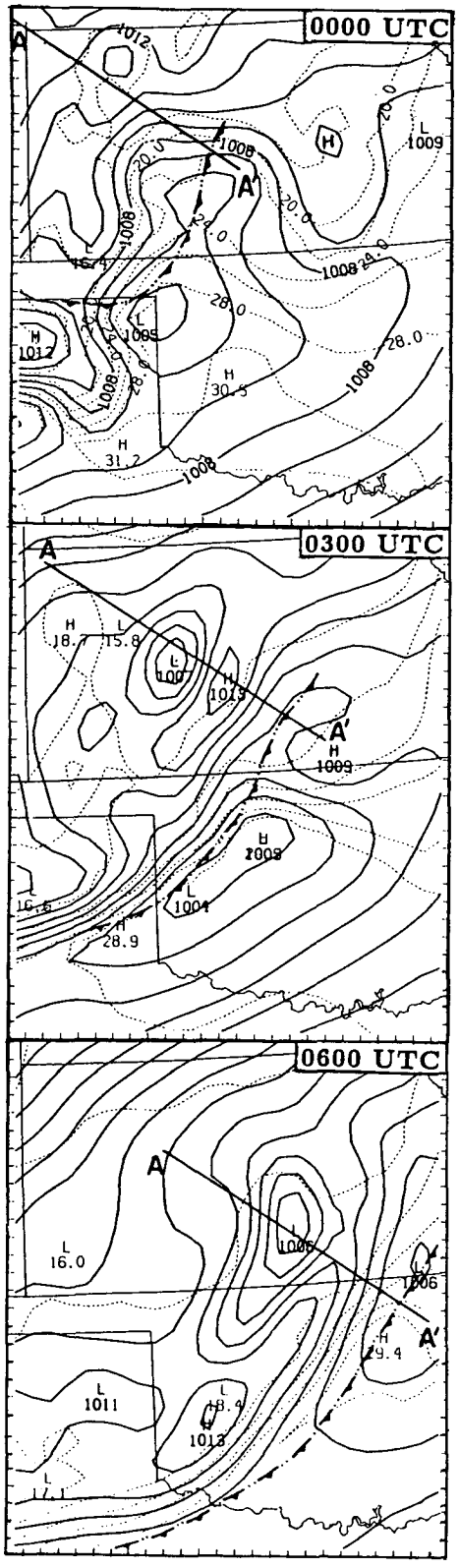

FIG. 1. The distribution of sea-level pressure (mb, solid lines) and surface temperature (°C, dashed lines) from 12, 15 and 18 h simulations, verified at 0000, 0300 and 0600 UTC 11 June 1985, respectively. The cold frontal symbols alternated with double dots indicate the leading convective line. The intervals marked on the frame are the fine-mesh grids (i.e., 25 km).

exhibit three distinct airflows within the system: a leading overturning updraft, an ascending FTR flow associated with the generation of the trailing stratiform precipitation, and an overturning downdraft associated with the rear-inflow jet (see Thorpe et al. 1982 for the definition of the terminology). Zhang and Gao found that this airflow structure is more or less determined by the distribution of geopotential height (see right panel in Fig. 2). In particular, the squall-induced surface mesohigh and a midlevel mesolow to the rear of the leading edge appear to force the development and evolution of the rear-inflow jet. They further showed that the surface wake low formed as a result of subsidence warming by descending air within the rear-inflow jet and can be indirectly linked to the development of the surface mesohigh about 150 km ahead. In the next two sections, we show how individual terms in the momentum equations contribute to the generation of these mesoβ-scale features.

Since various observational studies indicate different vertical transport behavior of horizontal momenta between the normal (U) and the parallel (V) components to the convective line (LeMone 1983; Zipser et al. 1981), there is a motivation to transform horizontal momenta from the model (x, y) coordinates into the right-handed coordinates (n, s) with n-axis normal to the line, positive in its direction of movement. To separate the advective effects associated with the system translation from the dynamical processes that influence the system development, a quasi-Lagrangian approach is adopted in which the budget is evaluated in coordinates following the leading edge. Furthermore, the flux form of the momentum equations in the σ-coordinates needs to be decoupled and transformed into the pressure coordinates for the purpose of comparing with other studies. Thus, the horizontal momentum equations in these transformed quasi-Lagrangian coordinates are given by

$$\frac{DU}{Dt} = -\mathbf{V}_h \cdot \nabla U - \omega \frac{\partial U}{\partial p} + fV - \frac{\partial \phi}{\partial n} + (F_{\mathrm{PBL}} + F_{\mathrm{DIF}})U, \quad (1)$$

$$\frac{DV}{Dt} = -\mathbf{V}_h \cdot \nabla V - \omega \frac{\partial V}{\partial p} - f(U + C) - \frac{\partial \phi}{\partial s} + (F_{\mathrm{PBL}} + F_{\mathrm{DIF}})V, \quad (2)$$

where $D/Dt = \partial/\partial t + C\partial/\partial n$, C is the system propagation speed normal to the leading line (i.e., 14.5 m s^{-1} along the direction of 125°) and the terms on the right hand side represent, respectively, the horizontal and vertical advection, the Coriolis force, the pressure

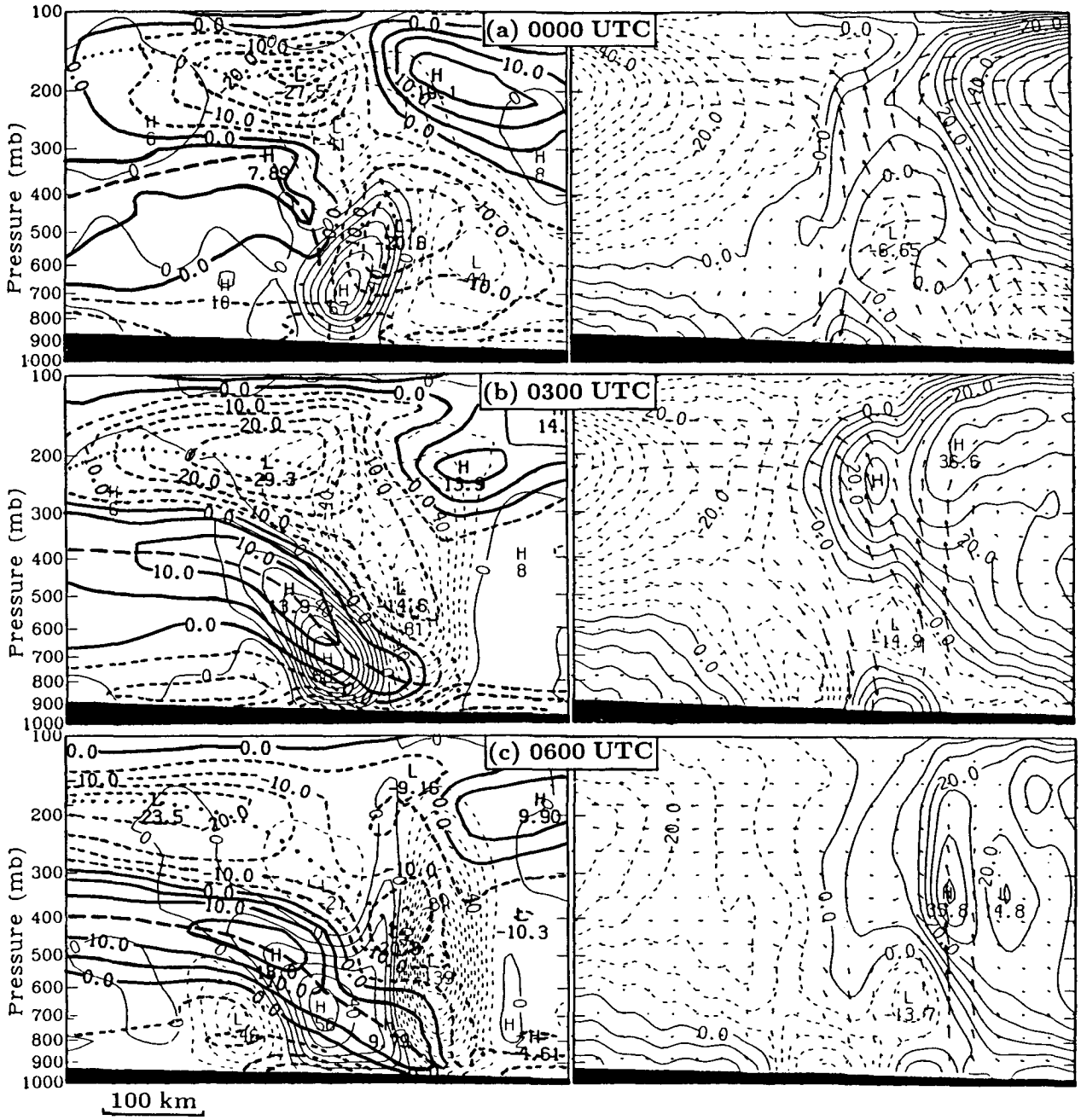

FIG. 2. Left panel shows the NW–SE vertical cross-sectional distribution of relative normal-line flow at intervals of 5 m s^{-1} (thick solid lines denote RTF flow and thick thin lines denote FTR flow), and vertical motion (ω, μb s^{-1}) at intervals of 10 μb s^{-1} from 12, 15 and 18 h simulations, verified at 0000, 0300 and 0600 UTC 11 June 1985, respectively. Right panel shows the corresponding distribution of relative circulation vectors normal to the line and height deviations (m). All solid (dashed) lines indicate positive (negative) values. Cross sections at individual times are taken along lines as given in Fig. 1 and cover a horizontal length of 475 km.

gradient force (generation term), boundary-layer processes and numerical diffusion. For the sake of simplicity, the horizontal advection term contains advection in both the along- and normal-line directions, i.e., $\mathbf{V}_h = U\mathbf{n} + V\mathbf{s}$. It should be pointed out that the subgrid-scale momentum parameterization in the Fritsch–Chappell convective scheme was excluded in the model integration. The possible consequence on the simulation and momentum budget results will be discussed in the final section.

The effects of convective momentum transport by mesoβ-scale circulations on the larger-scale mean flow

can be obtained following the conventional approach, i.e., by computing the vertical distribution or profiles of mesoβ-scale momentum fluxes: $\rho\overline{U'W'}$ and $\rho\overline{V'W'}$. Here the overbar denotes an average over a mesoβ-scale area that can include major mesoscale (convective) updrafts and downdrafts associated with the squall system, and U', V' and W' are deviations from their pressure-level averages. The vertical divergence of the fluxes then represents the contributions to the time rate of change in the larger-scale mean momentum due to the squall system.

3. Mesoβ-scale momentum budget normal to the line

In this and the next section, we will examine the generation of the mesoβ-scale structure and evolution of the June 10–11 squall circulation through the momentum transport and generation processes. All terms in Eqs. (1) and (2) can be evaluated directly from the model output.

a. Vertical cross-sectional distribution

Figure 3 shows the vertical cross section of relative horizontal advection, momentum generation, vertical advection and quasi-Lagrangian U-momentum tendency from the 12 h simulation (valid at 0000 UTC 11 June) along line $A-A'$ in Fig. 1. In order to facilitate understanding of the budget calculations, zero contours as well as axes of the maximum RTF and FTR relative flow, that appeared in Fig. 2, have also been superimposed. Other components in the budget equations are not displayed because, as will be shown later in this section, they are either relatively small (e.g., the numerical diffusion and boundary-layer terms) or linearly dependent upon the along-line flow (e.g., the Coriolis force). Note that since these cross sections are obtained from their instantaneous values, they may be influenced by fast propagating numerical Lamb waves.

At 0000 UTC 11 June, the simulated deep convection has nonuniformly formed along the leading line during the previous three hours and the rear inflow

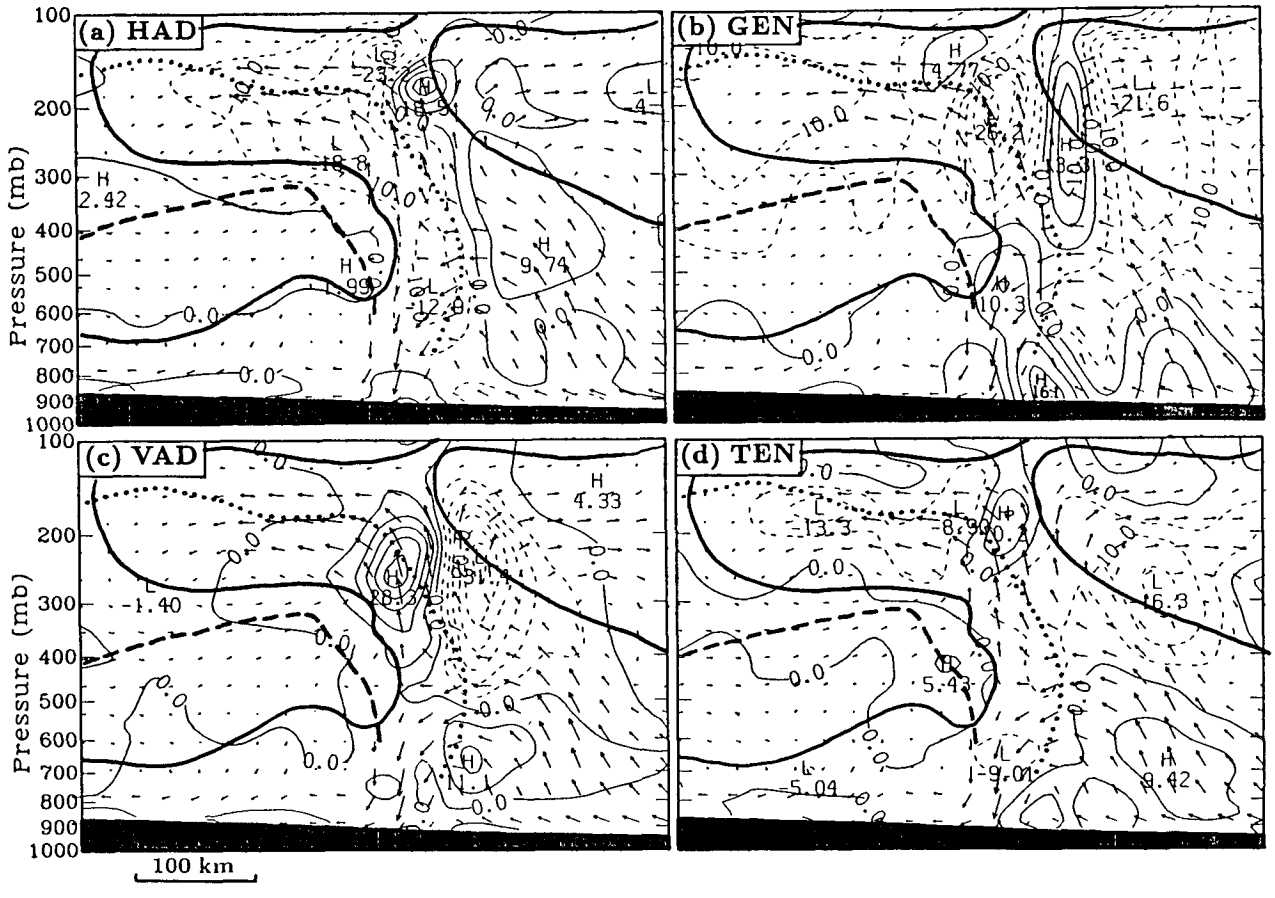

FIG. 3. The vertical cross section of (a) horizontal momentum advection ($-\mathbf{V}_h\cdot\nabla U$); (b) generation term ($-\partial\phi/\partial n$); (c) vertical momentum advection ($-\omega\partial U/\partial p$); and (d) quasi-Lagrangian momentum tendency (DU/Dt) at intervals of 5 m s^{-1} h^{-1} along line $A-A'$ in Fig. 1a from 12 h simulation, verified at 0000 UTC 11 June. The thin solid (dashed) lines indicate RTF (FTR) acceleration of the flow. The thick solid lines indicate interfaces between RTF and FTR flows and the thick dashed (dotted) lines indicate the axes of RTF (FTR) flow. Circulation vectors are also superposed.

tended to descend as it extended forward (Fig. 2). Although in many places the quasi-Lagrangian momentum tendency appears to be the result of small differences between large terms, in the regions of the trailing and descending rear inflow and the upper-level FTR outflow consistent areas of acceleration are clearly evident (Fig. 3). The maximum net accelerations of the RTF inflow and exiting FTR outflow are 5.4 and 8.9 m s^{-1} h^{-1}, respectively. These magnitudes are considered to be reasonable rates for the present case in which both the observed and simulated relative rear inflows and FTR outflows later attained values more than 15 and 25 m s^{-1}, respectively. Due to the use of the quasi-Lagrangian coordinate, the relative horizontal advection contributes little to the trailing rear inflow but very significantly to the ascending FTR flow. It is apparent that *the generation term provides the most significant contribution to the RTF acceleration and its downward extension*; its maximum rate of 16.1 m s^{-1} h^{-1} appears near the surface. This large generation rate coincides with the deepening of the surface mesohigh and pre-squall mesolow (cf. Figs. 1a, 2a and 3b). Clearly, the generation term is largely responsible for the subsequent development of the downward and forward extension of the rear inflow. This result is consistent with the conclusion drawn from a series of sensitivity tests by ZG that latent cooling through evaporation, melting and parameterized downdrafts primarily account for the generation of the descending portion of the rear inflow. Without any of these physical processes, the surface mesohigh and wake low are either weak or absent and the rear inflow fails to reach the surface.

The sign of the flow acceleration at the mid-to-upper levels is principally determined by the height perturbations. A large portion of the FTR pressure gradient force in the mid- to upper-levels is due to the presence of a coincident traveling mesoα-scale trough-ridge system (see Figs. 3 and 14 in ZGP) in the large-scale environment in which the squall line propagates. The presence of a weak warm-core-related mesohigh near the top of the leading updraft superposes a perturbation of the RTF acceleration ahead and FTR acceleration behind on the large-scale field. It is worth pointing out that in a sensitivity test in which the diabatic heating associated with moist convection was turned off, the upper-level FTR flow fails to develop (see Fig. 18 in ZG). This reveals that the background pressure gradient force is mostly balanced by the Coriolis force, and the upper-level FTR outflow results from a convectively generated pressure field. From Figs. 3a and b, the relative rearward advection and continuous momentum generation appear to be responsible for the rapid development of the upper-level FTR momentum during the incipient phase.

On the contrary, the vertical momentum advection produces substantial deceleration of both FTR and RTF outflows at the upper levels. This can be explained by the presence of negative vertical wind shears behind the leading updraft and positive shears ahead. Only when the FTR ascending flow leans increasingly towards the upshear direction, as will be seen in Fig. 4, can the vertical advection contribute to the rearward acceleration of the FTR flow. At the low levels, convectively generated updrafts also produce a deceleration of the FTR flow during this phase due to the presence of a strong FTR inflow that developed at the midlevel (Fig. 2). Thus, both the background momentum generation and vertical advection contribute to the weakening of the overturning updraft circulation (Figs. 3b–d). According to Rotunno et al. (1988), the weakening of the overturning updraft as the upper-level FTR outflow strengthens tends to cause the subsequent upshear tilt of the system. It should be noted that while the convective updrafts produced deceleration of the FTR flow in the low levels at about this time, it had a significant contribution to the development of the midlevel strong FTR flow prior to 0000 UTC through the upward transport of the large FTR momentum at the lower levels (not shown).

By 0300 UTC 11 June (i.e., 15 h into the integration), the simulated squall system has fully developed and the rear inflow has extended near the leading updraft (Figs. 1 and 2). During this mature stage, the isopleths of all terms in the momentum equation are well organized and oriented along the direction of the air flow (Fig. 4). The net result is that the quasi-Lagrangian tendency exhibits accelerations in the ascending FTR flow aloft and the descending RTF flow below, similar to the case observed by Sanders and Emanuel (1977) and LeMone (1983). According to Smull and Houze (1987a) and Rutledge and Houze (1987), the enhancement of the ascending FTR flow facilitates the transport of hydrometeors from the leading updrafts rearward for the generation of the trailing stratiform precipitation. The pressure gradient force is largely responsible for the generation of the FTR flow. The vertical momentum advection tends to accelerate the FTR flow ahead and above its axis, thus elevating the whole layer of the FTR flow. The horizontal momentum advection tends to have the opposite effect.

Similar to the 0000 UTC budget, the generation term dominates all other processes in strengthening the descending rear inflow. The maximum rate at this time exceeds 25 m s^{-1} h^{-1} near the surface, which again suggests the important role of the latent cooling below the latent heating in the development of descending rear inflow. In particular, such an enhanced forcing is consistent with the continued deepening of the surface mesohigh or cold pool immediately behind the line (cf. Figs. 1, 2 and 4). In the region behind the leading updraft and below the rear inflow axis, the generation term is nearly balanced by the downward transport of the midlevel RTF momentum except near the bottom boundary where the generation overcompensates the vertical advection so that mass convergence between the surface mesohigh and wake low increases with time during this period (see Figs. 15 and 16 in ZGP).

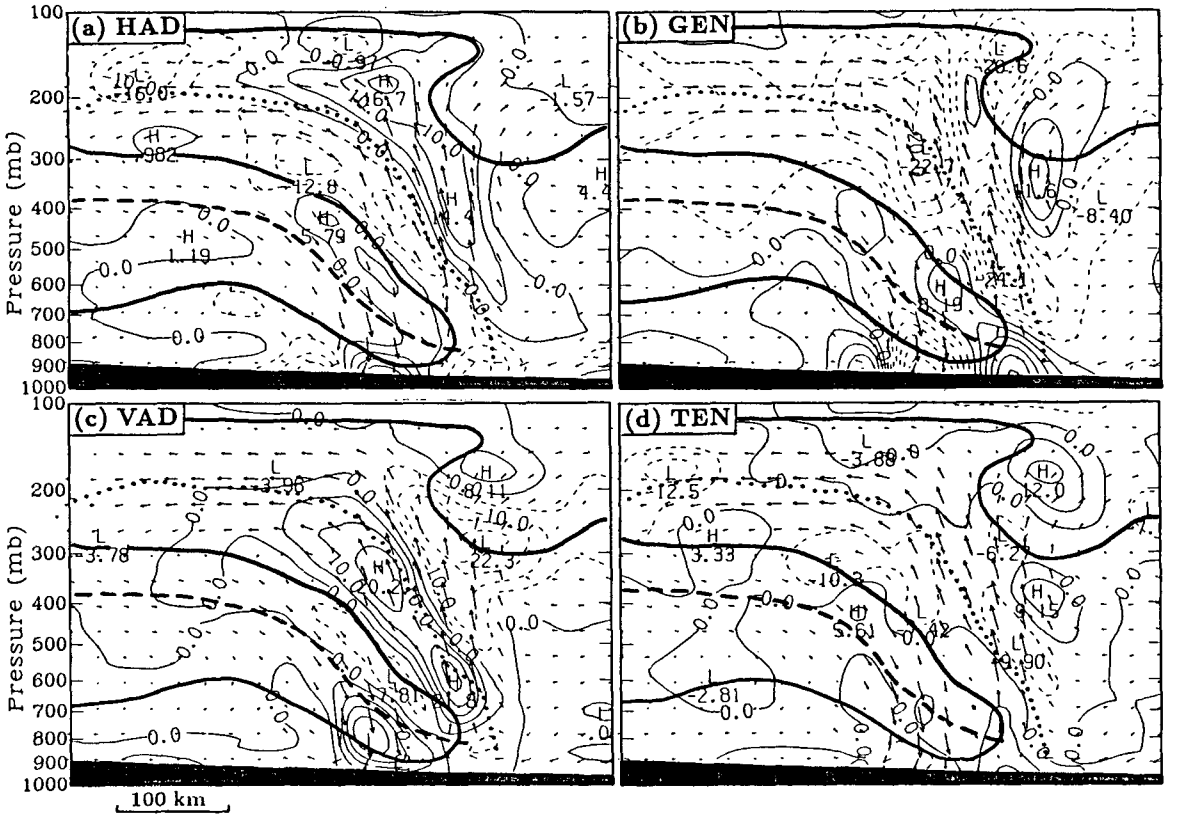

FIG. 4. As in Fig. 3 except from 15 h simulation, verified at 0300 UTC 11 June.

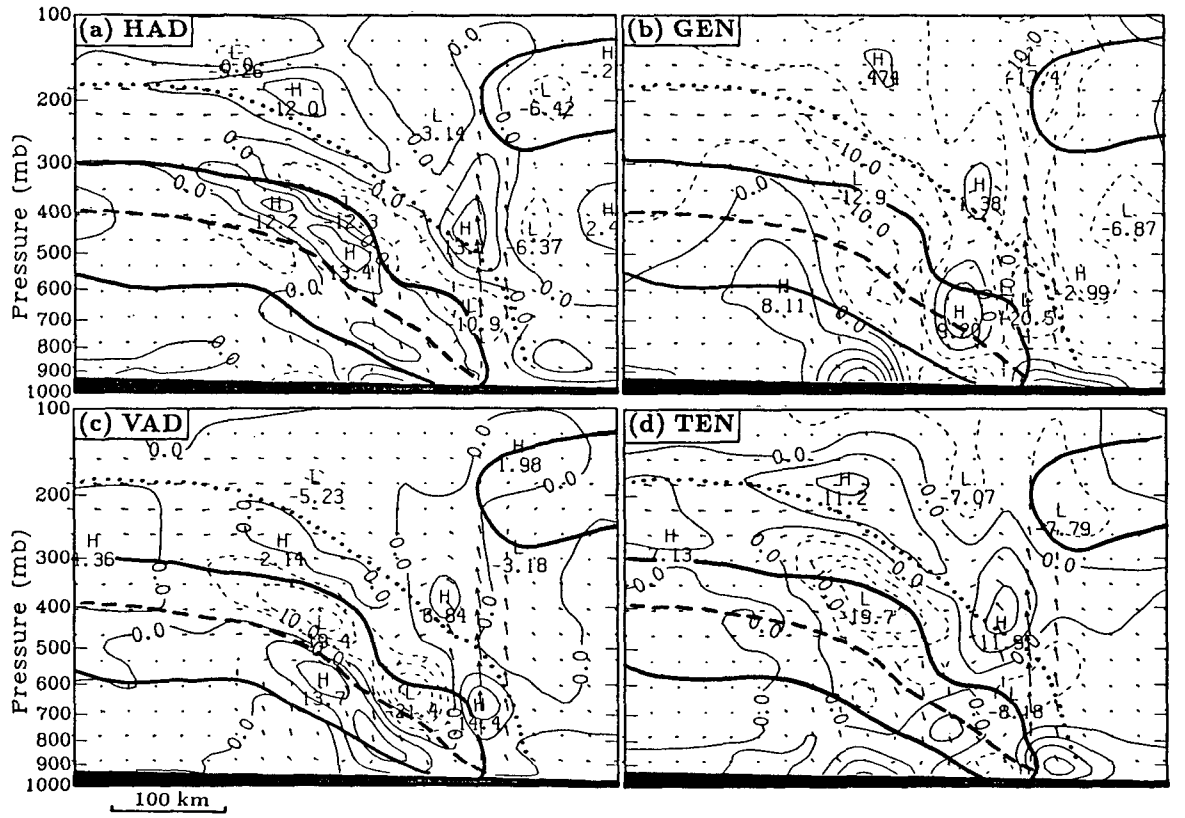

FIG. 5. As in Fig. 3 except from 18 h simulation, verified at 0600 UTC 11 June.

Although there was still a center of strong upward motion at 0600 UTC 11 June (i.e., 18 h into the simulation), as can be seen in Fig. 2, the simulated squall line rapidly dissipates hereafter as it progressively propagated into a more convectively stable environment (see ZGP). Thus, the momentum budget at 0600 UTC is appropriate for examining the demise of the squall system (Fig. 5). The strong upward motion and accompanying warm-core–related mesohigh at the upper levels are associated with the mesovortex that passes through the vertical cross section from the north (cf. Fig. 28 in ZGP and Fig. 2 herein). The overall distribution of the momentum generation exhibits a more weakly organized structure as compared to that a few hours earlier. For example, the generation of RTF acceleration behind the leading line tends to split into two centers: one ahead of the surface mesohigh that continues to propagate forward and another behind the rapidly diminishing midlevel mesolow. Likewise, the momentum generation in the mid-to-upper levels is basically dominated by the background pressure gradient force. The momentum generation still overwhelms all other terms in inducing the advancement of the descending rear inflow only at the lowest layers, since the cold pool is a stable structure. The disorganized distribution of the generation term can be clearly attributed to the decreases in the latent heat release, the fallout of precipitable water and latent cooling, in that order. The vertical momentum transport in the updrafts also becomes disorganized. In particular, the vertical advection no longer contributes significantly to the acceleration of the FTR ascending flow. As a result, the quasi-Lagrangian tendency displays a considerable deceleration in the FTR ascending flow and the disruption of the RTF acceleration in the rear inflow that eventually leads to the separation of the de-

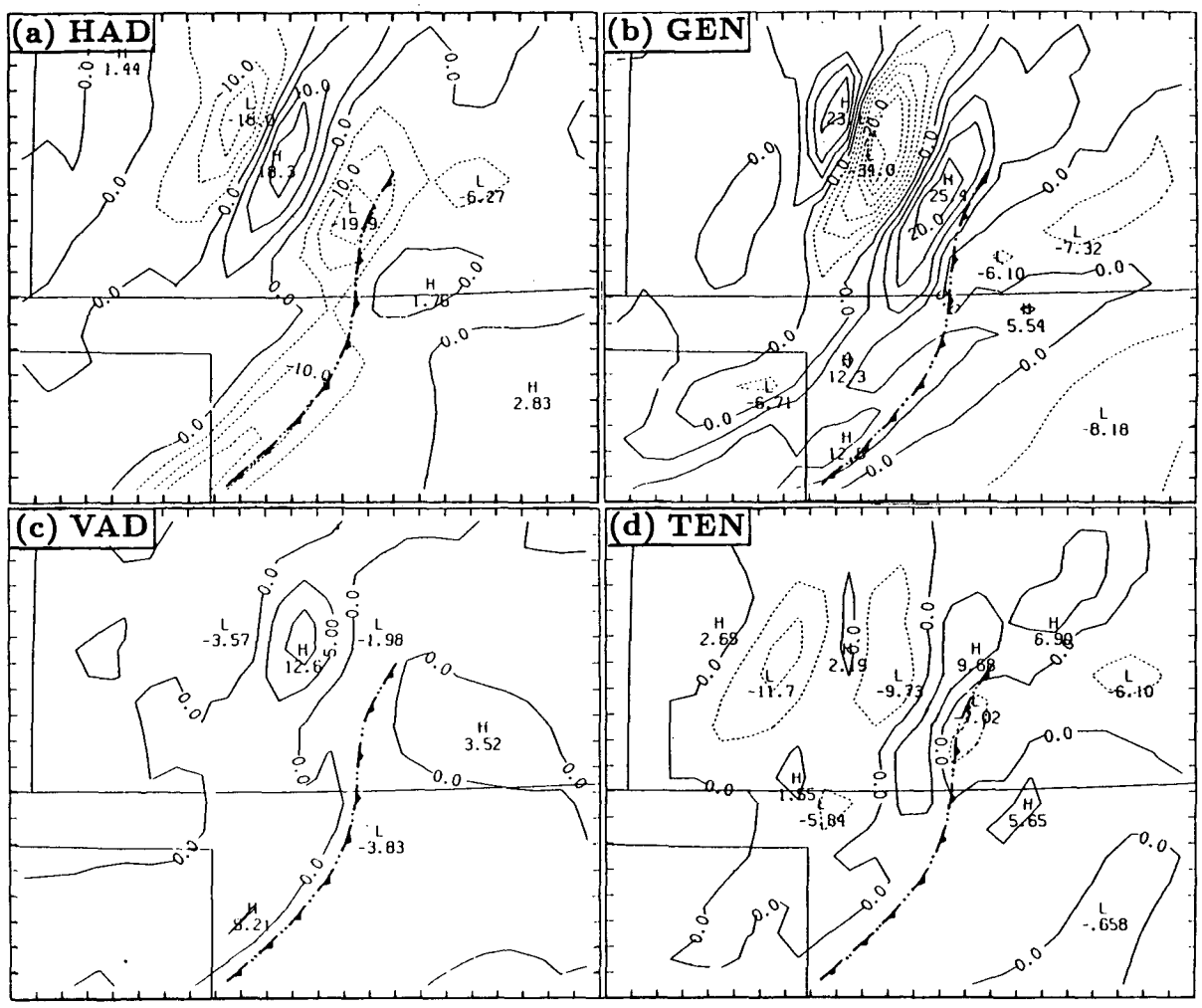

FIG. 6. The horizontal distribution of (a) horizontal momentum advection ($-\mathbf{V}_h \cdot \nabla U$); (b) generation term ($-\partial\phi/\partial n$); (c) vertical momentum advection ($-\omega \partial U/\partial p$); and (d) quasi-Lagrangian momentum tendency (DU/Dt) at intervals of 5 m s^{-1} h^{-1} at 900 mb from 15 h simulation, verified at 0300 UTC 11 June. The thin solid (dashed) lines indicate RTF (FTR) acceleration of the flow. The location of the leading convective line is denoted by cold frontal symbols alternated with double dots.

scending rear inflow from the surface counterpart (see Fig. 3c in ZG). It is interesting to note that all three of the terms contribute to the lowering of the FTR flow layer at the rear edge of the system during this stage.

b. Horizontal distribution

In order to show if the U-momentum budget results described in the previous subsection are representative of the entire squall line, Figs. 6–8 display the horizontal distribution of the momentum budget terms at 900, 600 and 250 mb levels during the mature phase. The location of the leading line of the squall line has also been indicated.

Although the most significant centers of maxima and minima in these diagrams are located over the northeastern portion of the squall system in association with the development of the mesovortex, well-defined SW–NE oriented perturbations are evident throughout all levels along and behind the line. In the lowest layer, the horizontal advection appears to be the primary process that offsets the momentum generation in determining the magnitude of the descending rear inflow. The vertical advection becomes a more dominant term in the midlevels in causing the RTF acceleration of U-momentum. The generation of the RTF flow through the pressure gradient force can be clearly seen, sloping upward from the leading line at 900 mb (Fig. 6b) to about 100 km behind the line at 600 mb (Fig. 7b). This slope is related to the tilted pressure distributions which exhibit pressure centers and horizontal gradients of opposite sign between the surface and midlevel. Note that the largest RTF acceleration occurs near the Oklahoma–Kansas border (Fig. 7d). This coincides with the radar observations by Rutledge et al. (1988) that showed a notch or bowlike echo structure over this region. Smull and Houze (1985) attributed this type of echo pattern to an intense rear inflow of dry air. As ZG showed, the intensification of the mesovortex plays an important role in the development of such strong descending rear inflow. Of particular interest, this large

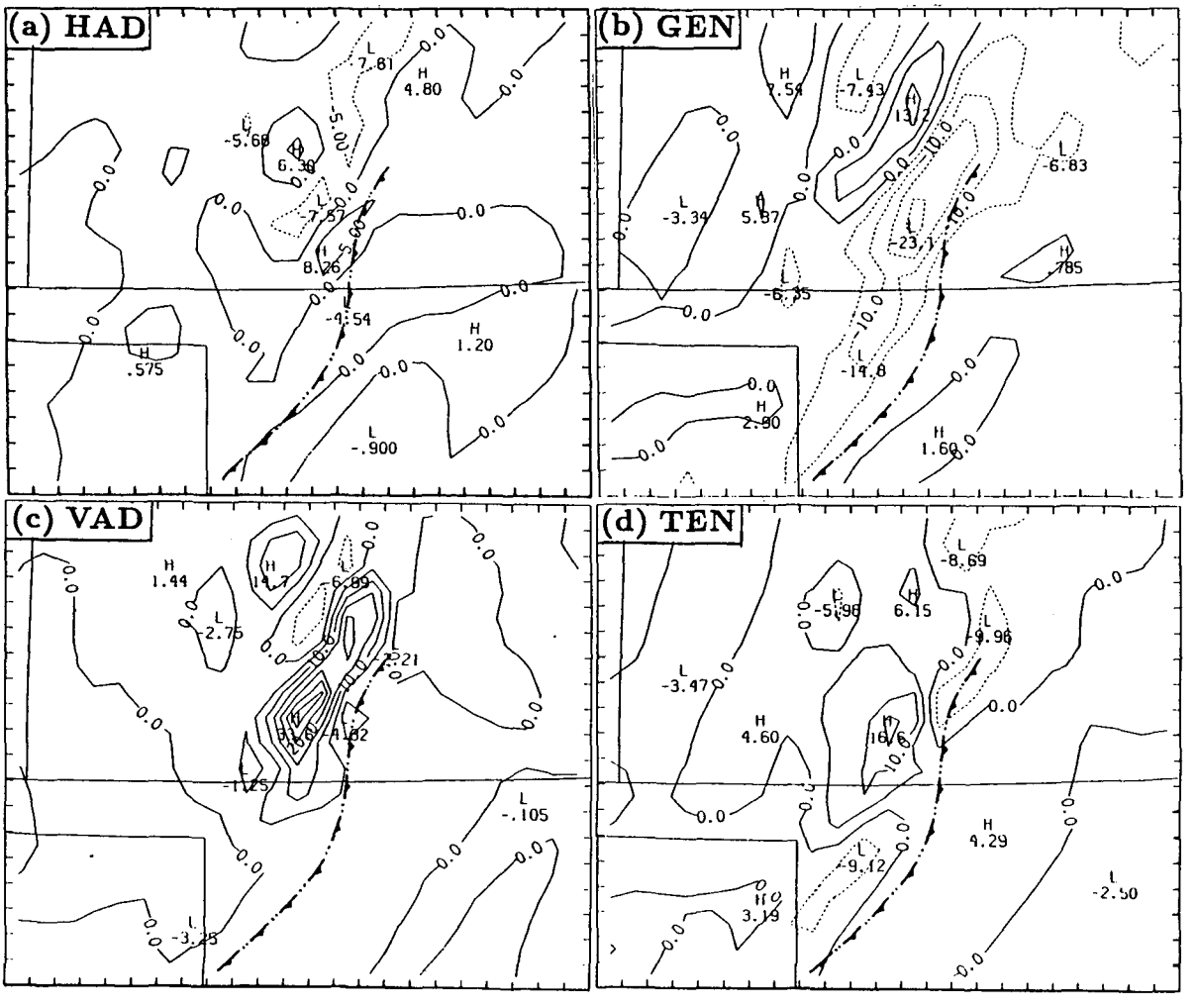

FIG. 7. As in Fig. 6 but for 600 mb.

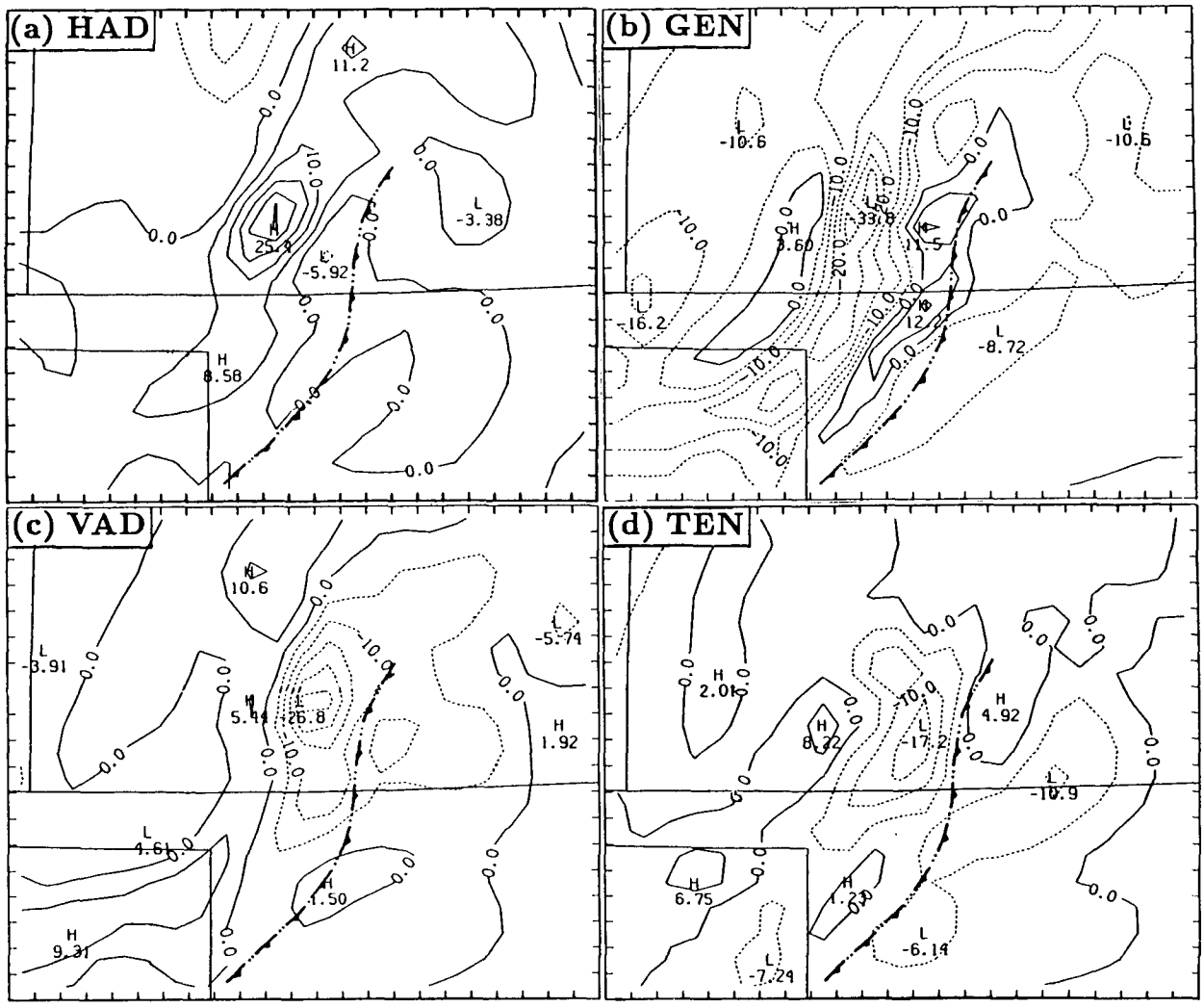

FIG. 8. As in Fig. 6 but for 250 mb.

RTF acceleration is dominated by the vertical momentum advection rather than the pressure gradient force since the midlevel mesolow is located about 100 km behind the leading line.

At the upper levels (i.e., 250 mb), both the generation and vertical momentum advection contribute to the net acceleration of the FTR flow over the stratiform region (Fig. 8). As discussed in the preceding subsection, this results primarily from the convectively generated mesohigh and the vertical transport of the midlevel FTR momentum. The horizontal momentum advection produces a well-defined band of the FTR deceleration at the back edge of the stratiform region.

c. *Composite vertical profiles*

To examine the relative importance of individual terms in Eq. (1), Figs. 9a and b show the composite vertical profiles of these terms taken at 40 and 80 km behind the leading line, respectively. These profiles are obtained by averaging the vertical distribution at six sequential grid points on both sides of the cross section $A - A'$ during the mature stage. It can be seen that contributions from the boundary-layer processes and numerical diffusion are negligible except at the lowest layers where a substantial amount of the horizontal momentum is lost to the ground through turbulent diffusion. Contribution from the Coriolis force is proportional to the along-line flow and has an amplitude the same order of magnitude as the generation and advection terms. Due to the orientation of the squall line, the Coriolis force produces a deceleration of the FTR momentum within the upper half of the troposphere with the maximum near the jet-stream level. This is consistent with the conjecture that the mean Coriolis force nearly balances the (large-scale) background pressure gradient force in the development of

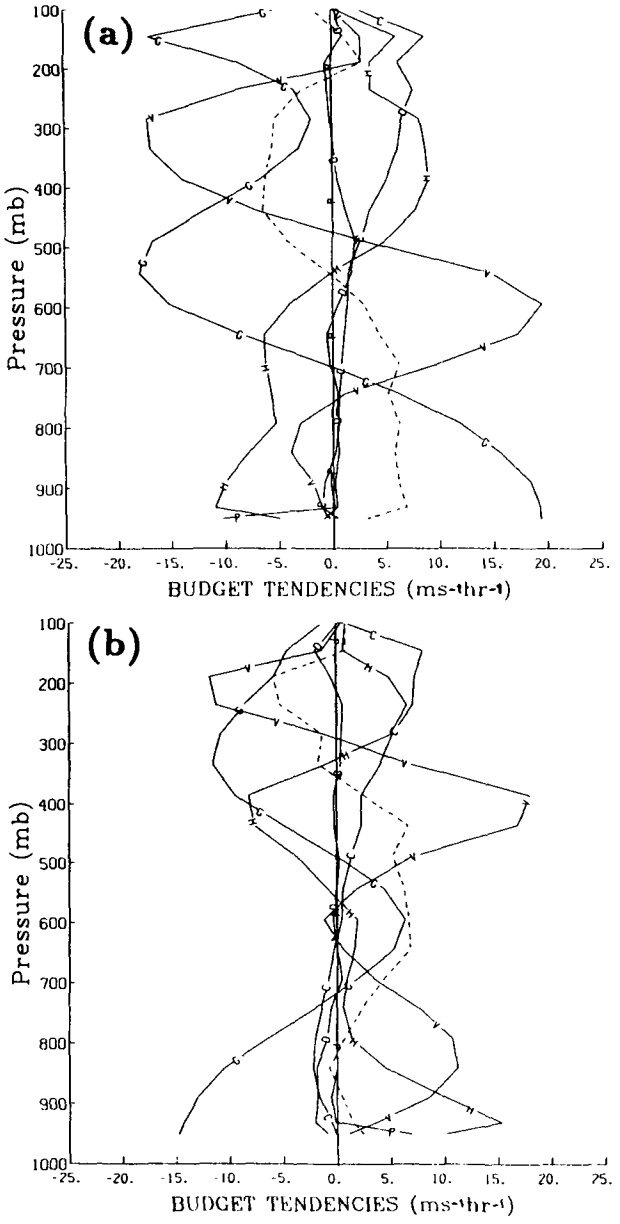

FIG. 9. Composite vertical profiles of individual terms in the U-momentum budget equation at (a) 40 km and (b) 80 km behind the leading line. The letter 'H' denote the horizontal momentum advection ($-\mathbf{V}_h \cdot \nabla U$); '$G$' the generation term ($-\partial\phi/\partial n$); '$V$' the vertical momentum advection ($-\omega\partial U/\partial p$); '$C$' the Coriolis force [$f(U+C)$]; '$P$' the boundary-layer effects ($F_{\mathrm{PBL}}U$); 'D' the numerical diffusion ($F_{\mathrm{DIF}}U$); and dashed lines denote the quasi-Lagrangian momentum tendency (DU/Dt) with a unit of m s^{-1} h^{-1} from the simulation around 15 h.

the upper-level FTR outflow, and thus the trailing stratiform precipitation.

As previously found, the momentum generation overcompensates all other terms in producing the RTF inflow, and creates the negative momentum tendency within the upper half of the troposphere. Generally, the peaks of the vertical momentum advection are lo-

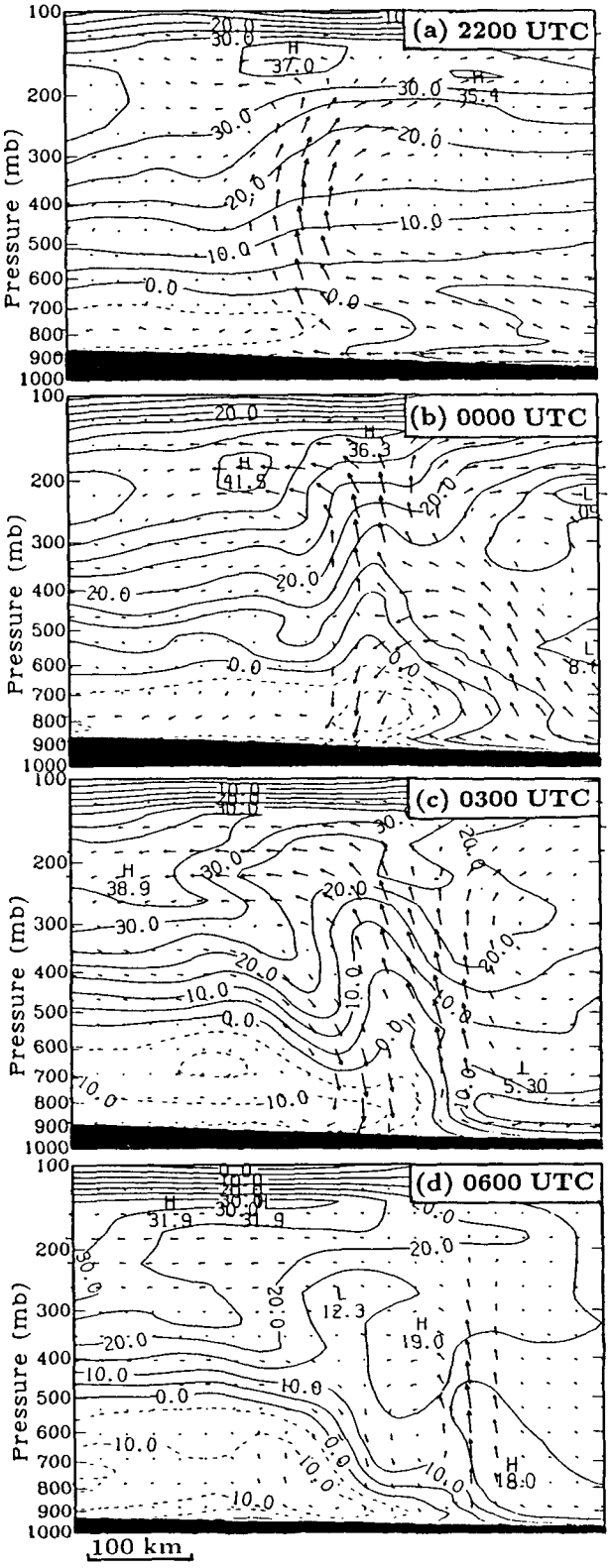

FIG. 10. Vertical cross section of the along-line (V) winds at intervals of 5 m s^{-1} from (a) 10 h, (b) 12 h, (c) 15 h and (d) 18 h simulations, verified at 2200, 0000, 0300 and 0600 UTC, respectively, along line $A - A'$ in Fig. 1. Vertical circulation vectors normal to the line are also superposed.

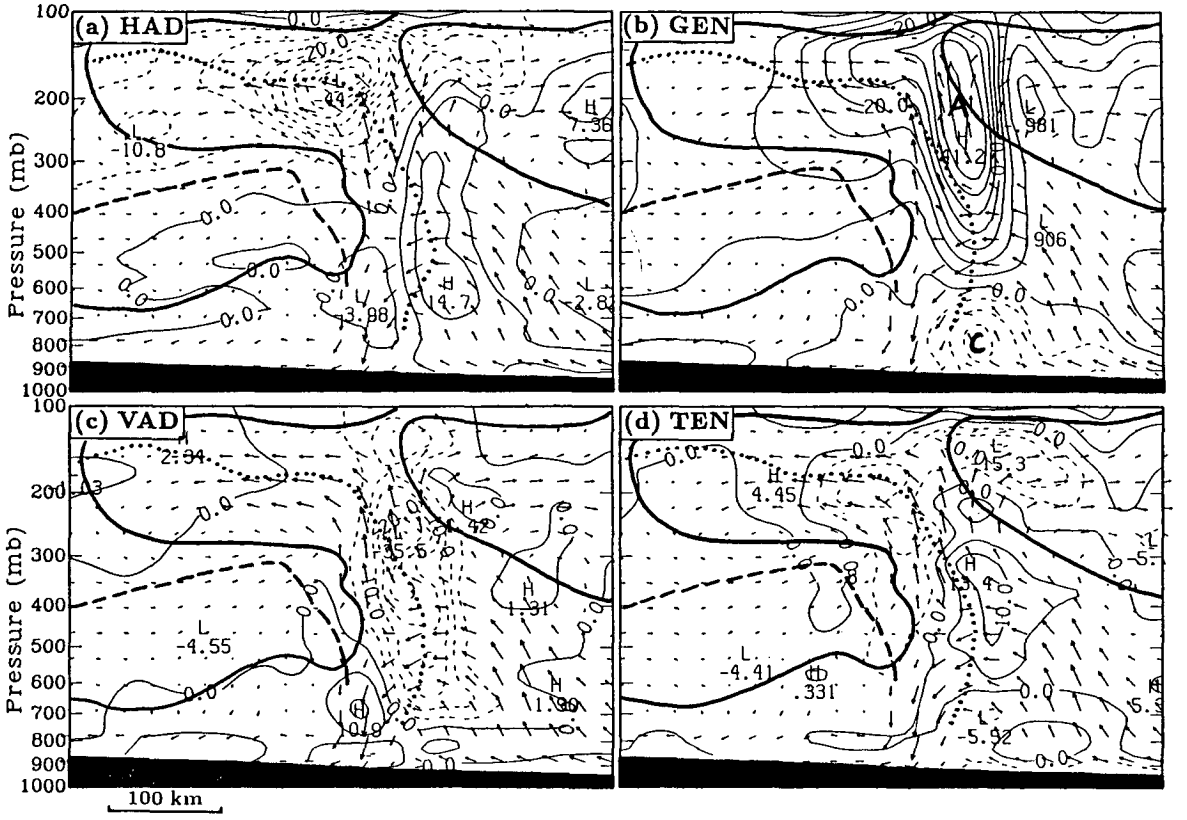

FIG. 11. As in Fig. 3 but for V-momentum budget. Thin solid (dashed) lines indicate flow into (out of) the page. Letters 'C' and 'A' denote the maximum tendencies of cyclonic and anticyclonic circulations.

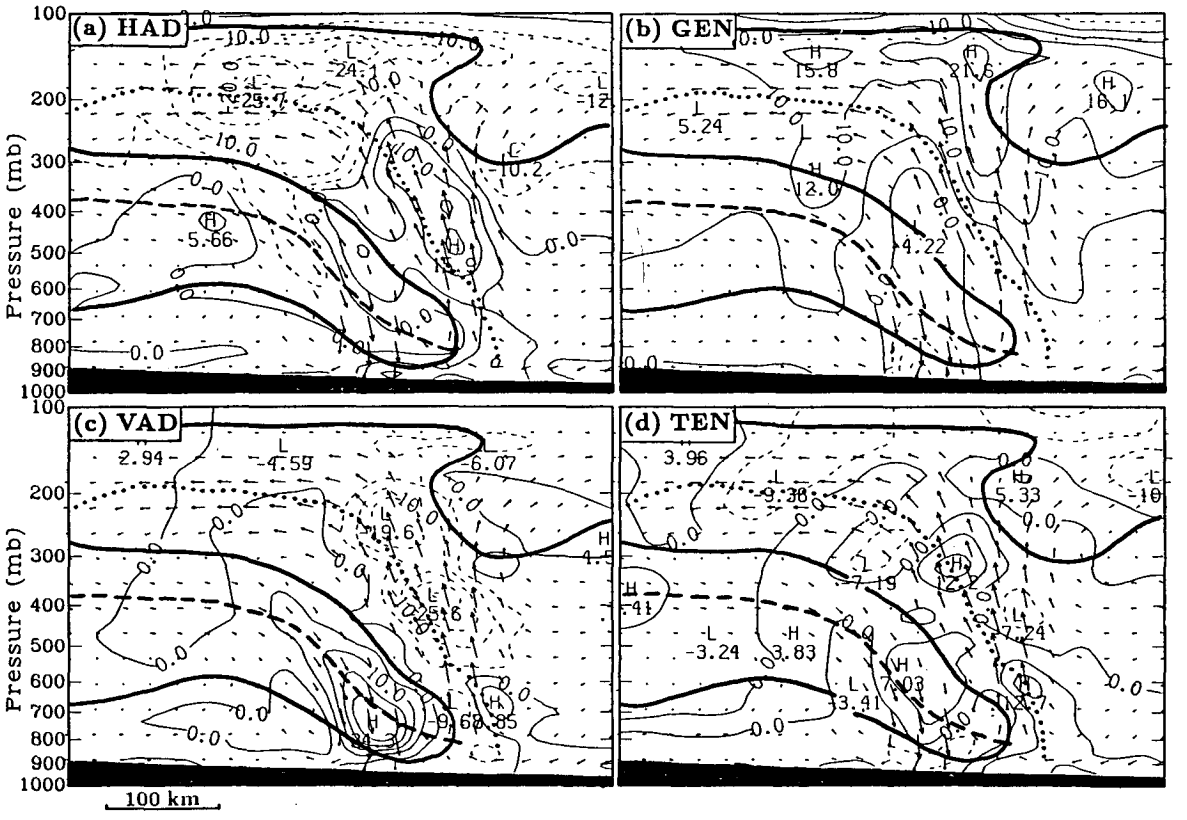

FIG. 12. As in Fig. 4 but for V-momentum budget. Thin solid (dashed) lines indicate flow into (out of) the page.

cated at levels above the levels of maximum momentum generation, again indicating that convectively generated updrafts tend to elevate the generated (FTR or RTF) flow layers. Note that the vertical variations in the horizontal and vertical momentum advection are nearly opposite in sign at most levels. This implies that the horizontal momentum advection tends to counteract the vertical momentum advection in the development of the squall line circulation. Overall, the squall line attains a net FTR acceleration aloft and a net RTF acceleration below, which in the present case clearly imposes a deceleration on the larger-scale mean flow.

4. Mesoβ-scale momentum budget parallel to the line

Since both ZGP and ZG showed that the June 10–11 squall line was three dimensional in nature due to the presence of the mesovortex at the northeastern portion of the system, we are motivated to examine the relative importance of the along-line generation versus advective processes in affecting the circulation of the squall system. First, let us inspect the cross-sectional evolution of the flow parallel to the line from the 10, 12, 15 and 18 h simulations, valid at 2200, 0000, 0300 and 0600 UTC, respectively (Fig. 10). Initially, the along-line flow is relatively uniform in the horizontal although there is strong shear in the vertical. Later, the structure of the flow is significantly distorted as the MCS's internal circulation develops. Near the end of the MCS's lifecycle, the along-line flow becomes approximately constant along stream lines, which tends to support the convective mixing concept discussed by Zipser et al. (1981) and LeMone (1983).

Figures 11–13 show the cross-sectional distributions of the V-momentum budget terms at different phases. During the incipient stage, there was a NE–SW acceleration (i.e., out of the page) in the lower levels and a SW–NE acceleration (i.e., into the page) in the upper levels behind the leading line (Fig. 11b); the maximum rate exceeds 40 m s^{-1} h^{-1}! This suggests the subsequent intensification of a cyclonic circulation overlaid by an anticyclonic circulation associated with the development of a midlevel warm-core structure (see Figs. 4 and 7 in ZG). However, such a large V-momentum generation is considerably compensated by the horizontal and vertical momentum advection. Since the magnitude of the along-line flow increases with height, convectively generated updrafts tend to decelerate the flow at higher levels whereas convective downdrafts

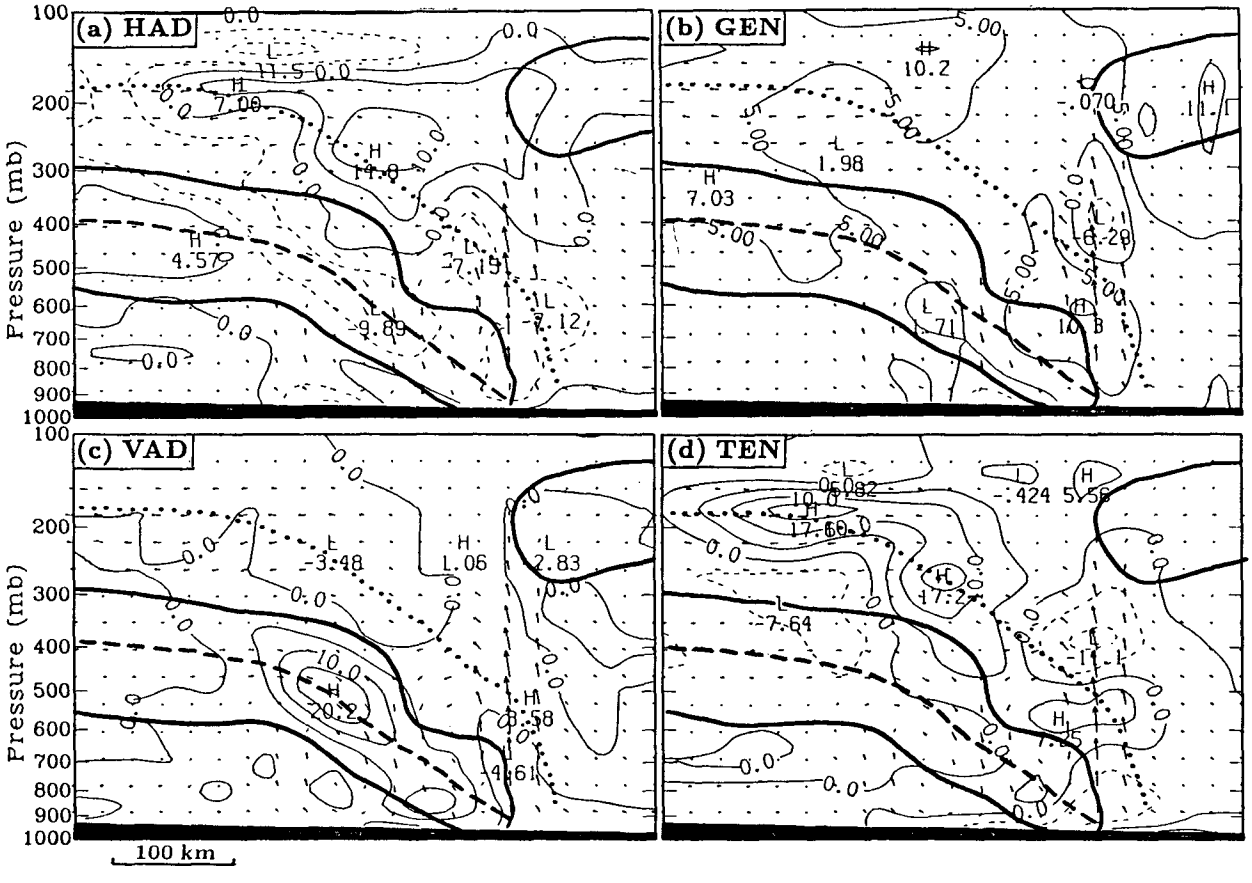

FIG. 13. As in Fig. 5 but for V-momentum budget. Thin solid (dashed) lines indicate flow into (out of) the page.

accelerate the flow at lower levels, particularly at a later stage, thus reducing the vertical wind shear. The horizontal momentum advection contributes to the deceleration of the upper-level flow due to the superposition of the anticyclonic circulation ahead of the jet stream (cf. Figs. 10 and 11).

At 0300 UTC 11 June, although the generation term still contributes to the enhancement of the low-level cyclonic circulation and the upper-level anticyclonic circulation, its magnitude becomes much smaller compared to three hours earlier (Fig. 12). The mesovortex circulation is then primarily maintained through the inertial stability of large cyclonic vorticity (see Zhang and Fritsch 1987). Note that at this time the background pressure gradient parallel to the line is almost negligible, compared to the normal-line component. In contrast, both the vertical and horizontal momentum transports are well organized and dominate the V-momentum tendency; the transport of momentum is downgradient. The V-momentum generation during the dissipation period nearly vanishes over the entire cross section, and all other terms except for the Coriolis force are weakly organized (Fig. 13). These results suggest that the momentum generation parallel to the line only provides an important contribution to the initial intensification of the horizontal rotational flow in this particular case but has little effect on the final vertical structure of the along-line flow. It is necessary to mention that a vertical cross section taken at the southwest portion of the line also exhibits a weakly organized distribution of the along-line momentum generation and a reasonably organized transport structure of the V-momentum during the MCS's lifecycle. This further reveals *the dominant roles of convectively generated vertical transports in determining the structure of horizontal flow along the line*. If this is the case, the momentum transport parallel to the line can be qualitatively understood according to mixing length or K theory, as mentioned by LeMone (1983) and LeMone et al. (1984).

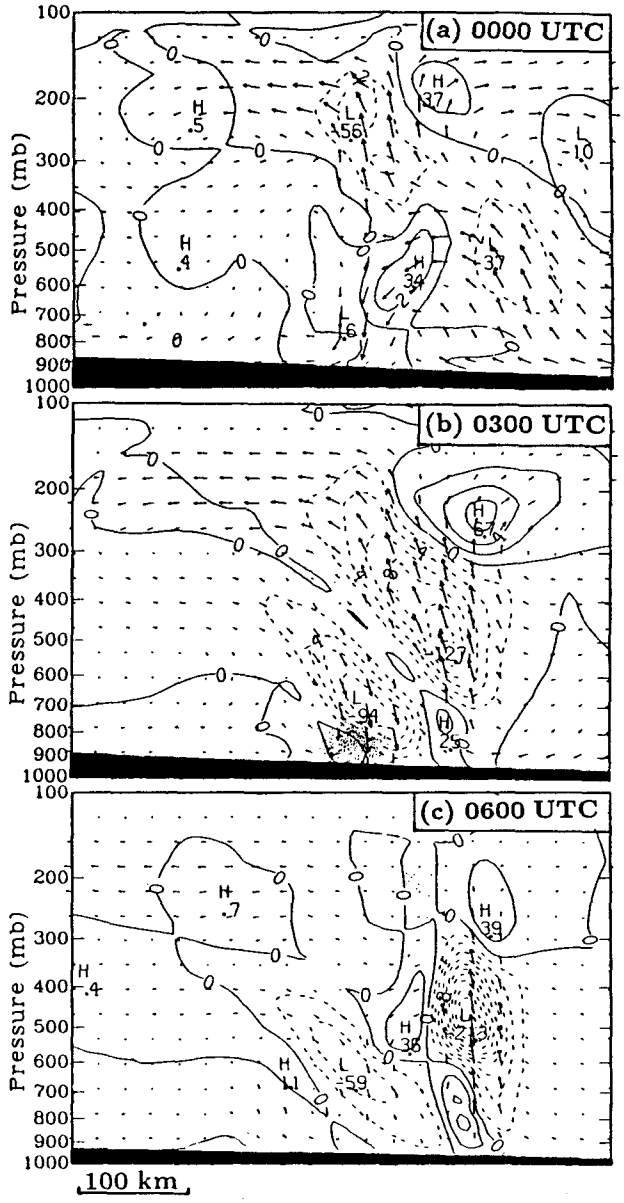

FIG. 14. Vertical cross section of U-momentum flux ($\rho U'W'$) at intervals of 2 kg m^{-1} s^{-2} from (a) 12 h, (b) 15 h and (c) 18 h simulations along line $A - A'$ in Fig. 1. All solid (dashed) lines denote positive (negative) values. Vertical circulation vectors normal to the line have been superposed.

5. Integral effect of momentum flux on the mean flow

In this section, the integral effects of vertical momentum transport are estimated by considering the convectively generated mesoβ-scale circulations and momentum perturbations (deviations) as submesoα-scale processes.

Figure 14 shows the vertical cross-sectional distribution of $\rho U'W'$, the eddy momentum flux normal to the line from the 12, 15 and 18 h simulations, valid at 0000, 0300 and 0600 UTC 11 June, respectively. It is apparent that the vertical motion (W, m s^{-1}) and momentum deviations are negatively correlated during most phases. In other words, the eddy U-momentum flux is consistently negative over most portions of the ascending FTR flow and descending RTF flow, except for 0000 UTC when the midlevel low-θ_e air ahead of the leading line is forced to descend rearward and produces a positive momentum flux. This implies that convectively generated updrafts are carrying FTR momentum and increase momentum aloft in the direction opposite to the movement of the system whereas the convectively generated downdrafts are carrying RTF momentum downward. This is most pronounced when the MCS tilts increasingly in the upshear direction. In fact, within the upper portion of the overturning updraft, positive U-momentum flux occurs. It is impor-

tant to point out that *moist downdrafts play as crucial a role as convectively generated updrafts in transporting horizontal momentum*. Moreover, the effects of moist downdrafts in both convective and stratiform regions are of equal importance. This is in marked contrast with the results obtained by LeMone (1983) and LeMone et al. (1984) for tropical squall lines in which moist downdrafts are relatively weak.

Figure 15 displays the area-averaged (over the northern half portion of the squall system) vertical profiles of the relative U-wind and U-momentum flux ($\rho\overline{U'W'}$). Initially, the FTR flow appears at almost all the levels with its maximum at 500 mb. Later, the larger-scale response to the convective development results in an enhancement of the upper-level FTR flow and the generation of the RTF flow at the midlevel. This process can be explained by the vertical profiles of the U-momentum flux, which shows negative values continuously with its minimum varying from the initial 300 mb level to the 500 mb level at later times. The vertical divergence of the U-momentum flux then produces a continued acceleration of the larger-scale FTR and RTF mean flows at, respectively, the upper and lower levels, and an increase in the vertical U-wind shear. Thus, deep convection tends to transport the U-momentum countergradient, as found in the studies by LeMone (1983) and Moncrieff (1981). From the foregoing mesoβ-scale budget calculations, this is evidently due to processes associated with the momentum generation normal to the line.

In contrast, the distribution of V-momentum flux ($\rho\overline{V'W'}$) shows that the correlation between vertical motion and V-momentum deviations is dependent on the *local vertical shear* along the line (cf. Figs. 10 and 16). Specifically, deep convection tends to transport V-momentum downgradient so as to reduce the vertical shear, as mentioned before. This is fundamentally distinct from that normal to the line. The downgradient transport property can be better seen from the corresponding composite vertical profiles. Figure 17 shows that the lower troposphere sustains a continuous acceleration of the along-line flow while at the upper portion of the troposphere there is a deceleration. The acceleration and deceleration are clearly due to the dominant role of moist downdrafts and convectively generated updrafts, respectively. These results again support previous observational studies by Zipser et al. (1981), LeMone (1983) and LeMone et al. (1984).

6. Discussion

In the present momentum budget study, we have shown that the pressure gradient force normal to the line is dominant in the momentum budget and essentially determines the mesoβ-scale structure and evolution of the MCS.

As mentioned in section 2, this budget study is based on a numerical simulation in which convective cells are represented by the Fritsch–Chappell parameterization with the subgrid-scale momentum transport excluded. A question naturally arises whether the momentum budget would be substantially different if an appropriate convective momentum parameterization was included. We have shown that in the present case

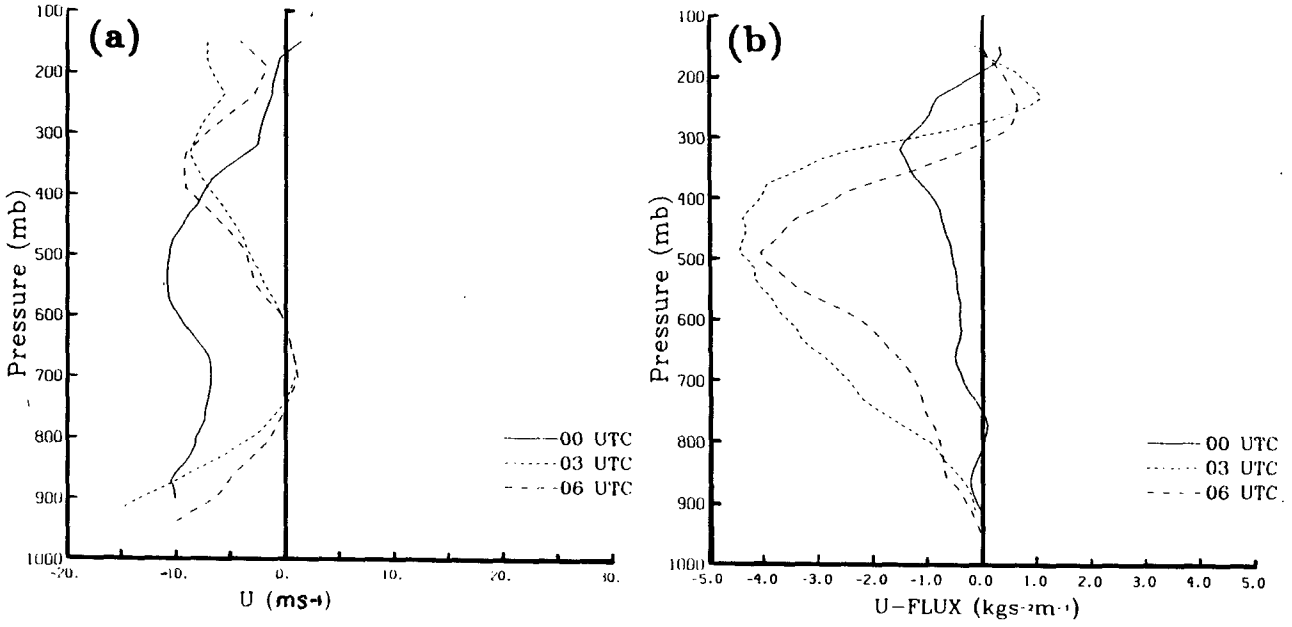

FIG. 15. Vertical area-averaged profiles of (a) relative winds normal to the line and (b) U-momentum flux ($\rho\overline{U'W'}$). The profiles are obtained by averaging the corresponding variable over an area of 475 km × 300 km in the northern portion of the squall system.

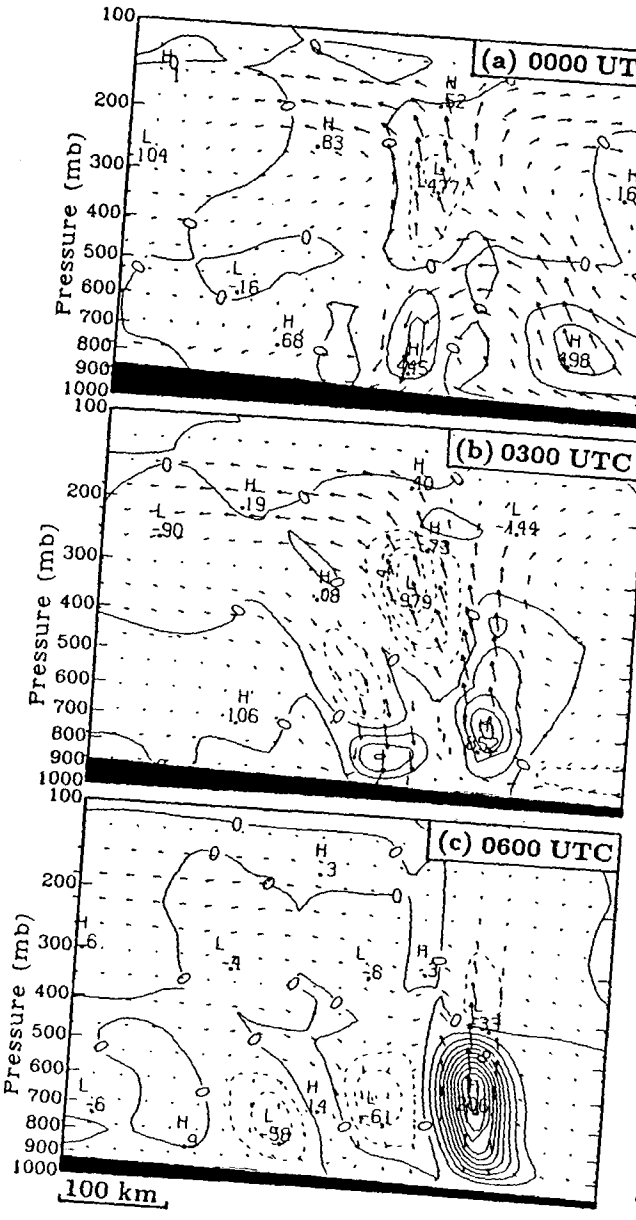

FIG. 16. As in Fig. 14 but for V-momentum.

the maximum resolvable-scale momentum generation rates for both the front-to-rear and rear-to-front flows exceed 25 m s^{-1} h^{-1}. This is about one order of magnitude larger than could be obtained by any known type of cumulus momentum parameterization. For example, with the subgrid-scale horizontal pressure gradients taken into account, Flatau and Stevens (1987) estimated a peak rate of about 3–4 m s^{-1} h^{-1} momentum changes across the convective portion of a tropical squall line (see their Figs. 12 and 13) on a grid scale of 30 km. Even for typical intense midlatitude cumulonimbus with strong wind shears, such as those analyzed by LeMone et al. (LBFT 1988) during the 1981 Cooperative Convective Experiment (CCOPE), the effect of the subgrid-scale pressure gradient was at most two to three times larger than the tropical counterpart. Under weak shear environmental conditions, the subgrid-scale momentum generation would be much less [LeMone et al. (LTB) 1988]. Thus, the effect of the subgrid-scale momentum transport on the dynamics of the present MCS can be considered to be of secondary importance, as compared to the parameterization of the thermodynamic effects. In this regard, Moncrieff (1978) provided an example with an analytical model in which varying the juxtaposition of a heat source and a heat sink in a sheared flow can result in considerably different internal flow structures for a MCS-like system. It is apparent that in the present case, the incorporation of moist downdrafts in the Fritsch–Chappell scheme and the use of the explicit moisture package are crucial for obtaining the successful simulation of the squall events. Nevertheless, we feel that the inclusion of the subgrid-scale momentum transport into the present simulation may sharpen the descent of the leading rear inflow in the neighborhood of the leading convective region of the MCS as observed by Rutledge et al. (1988) and Smull and Houze (1987b).

The along-line momentum budget reveals that the momentum parallel to the line can be considered as a conservative quantity. Although the incorporation of a convective momentum parameterization into the present model based on this concept may help improve the simulation of the along-line flow, it would have little effect on the structure and evolution of the squall system normal to the line which is our primary concern. In fact, when the parameterized momentum flux in the Fritsch–Chappell scheme was turned on, it produced much less impact on the simulation than the neglect or changes in any of the other physical processes (e.g., the surface heating, boundary-layer formulation, and needless to say, the explicit moisture).

The quantification of the importance of moist downdrafts in the momentum transport is another significant aspect of this study. The results indicate that the model treatment of moist downdrafts is a key element not only in predicting summertime, mid-latitude MCSs but also for obtaining the reasonable structure of horizontal momenta for these systems. Sensitivity tests, in which different moist-downdraft physics was omitted sequentially while holding other conditions the same as the control run, also support this conclusion (see Zhang and Fritsch 1988; Zhang et al. 1988; Zhang and Gao 1989). Zhang and Gao (1989) discussed the different roles the resolvable-scale and parameterized moist downdrafts play in the development of the descending rear inflow.

The budget study presented herein can be criticized on the ground that it is only based on a single case study and a numerical simulation in which various approximations are made. In particular, the 10–11 June MCS developed in a baroclinically influenced, midlat-

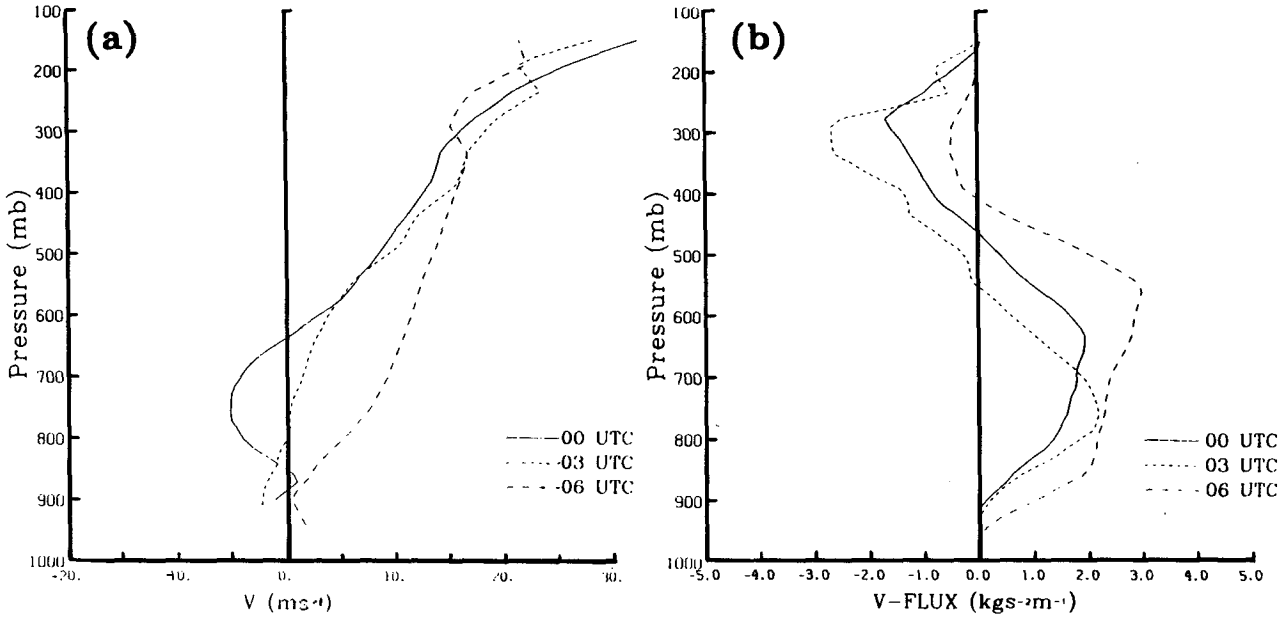

FIG. 17. As in Fig. 15 but for V-momentum.

itude environment with conditions favorable for generating strong moist downdrafts (see Zhang and Gao 1989), and this study represents the first effort to obtain the detailed momentum budget for this type of the system. Thus, further budget studies with high-resolution (observed) data cases are necessary. Nevertheless, the present MCS exhibits many of classic squall-line characteristics, as shown by Zhang et al. (1989) and Zhang and Gao (1989), and thus the results are quite representative of MCSs behavior. Moreover, Moncrieff (1981, 1989) showed that the momentum transport by the resolvable-scale processes of the type considered herein has a physical basis and is one of a hierarchy of momentum transport regimes.

Acknowledgments. We are grateful to Peggy LeMone for her helpful discussion and critical review of this manuscript, and to Bruce Albrecht and an anonymous reviewer for their useful comments. This research was completed at Division of Mesoscale and Microscale Meteorology, National Center for Atmospheric Research which is sponsored by National Science Foundation, and the preparation of the manuscript was carried out at Department of Physics, University of Toronto. The computations were performed on NCAR's CRAY X-MP.

REFERENCES

Anthes, R. A., E.-Y. Hsie and Y.-H. Kuo, 1987: Description of the Penn State/NCAR mesoscale model version 4 (MM4). NCAR Tech. Note, NCAR/TN- 282, 66 pp.

Augustine, J. A., and E. J. Zipser, 1987: The use of wind profilers in a mesoscale experiment. *Bull. Amer. Meteor. Soc.*, **68**, 4–17.

Chang, C.-B., D. J. Perkey and C. W. Kreitzberg, 1981: A numerical case study of the squall line of 6 May, 1975. *J. Atmos. Sci.*, **38**, 1601–1615.

Cho, H.-R., 1985: Rates of entrainment and detrainment of momentum of cumulus clouds. *Mon. Wea. Rev.*, **113**, 1920–1932.

Cunning, J. B., 1986: The Oklahoma–Kansas Preliminary Regional Experiment for STORM-Central. *Bull. Amer. Meteor. Soc.*, **67**, 1478–1486.

Flatau, M., and D. E. Stevens, 1987: The effect of horizontal pressure gradients on the momentum transport in tropical convective lines. Part I: The results of the convective parameterization. *J. Atmos. Sci.*, **44**, 2074–2087.

Fritsch, J. M., and C. F. Chappell, 1980: Numerical prediction of convectively driven mesoscale pressure systems. Part I: Convective parameterization. *J. Atmos. Sci.*, **37**, 1722–1733.

——, and R. A. Maddox, 1981: Convectively driven mesoscale weather systems aloft. Part I: Observations. *J. Appl. Meteor.*, **20**, 9–19.

Johnson, R. H., and P. J. Hamilton, 1988: The relationship of surface pressure features to the precipitation and air flow structure of an intense midlatitude squall line. *Mon. Wea. Rev.*, **116**, 1444–1472.

Kaplan, M. L., J. W. Zack, V. C. Wong and J. J. Tuccillo, 1982: Initial results from a mesoscale atmospheric simulation system and comparisons with the AVE-SESAME I dataset. *Mon. Wea. Rev.*, **112**, 2212–2238.

LeMone, M. A., 1983: Momentum transport by a line of cumulonimbus. *J. Atmos. Sci.*, **40**, 1815–1834.

——, G. M. Barnes and E. J. Zipser, 1984: Momentum flux by lines of cumulonimbus over the tropical oceans. *J. Atmos. Sci.*, **41**, 1914–1932.

——, ——, J. C. Fankhauser and L. F. Tarleton, 1988: Perturbation pressure fields measured by aircraft around the cloud-base updraft of deep convective clouds. *Mon. Wea. Rev.*, **116**, 313–327.

——, L. F. Tarleton and G. M. Barnes, 1988: Perturbation pressure at the base of cumulus clouds in low shear. *Mon. Wea. Rev.*, **116**, 2062–2068.

Maddox, R. A., D. J. Perkey and J. M. Fritsch, 1981: Evolution of

upper- tropospheric features during the development of a mesoscale convective complex. *J. Atmos. Sci.*, **38,** 1664–1674.

Matsumoto, S., 1972: Unbalanced low-level jet and solenoidal circulation associated with heavy rainfalls. *J. Meteor. Soc. Japan,* **49,** 267–281.

Moncrieff, M. W., 1978: The dynamical structure of two-dimensional steady convection in constant vertical shear. *Quart. J. Roy. Meteor. Soc.,* **104,** 543–567.

——, 1981: A theory of organized steady convection and its transport properties. *Quart. J. Roy. Meteor. Soc.,* **107,** 29–50.

——, 1985: Convective momentum transport. *Proc., Seminar Series on Phys. Param. of Numerical Models of the Atmos.,* ECMWF, Reading, 181–203.

——, 1989: Dynamical models of the transport of momentum, mass and inert tracers by mesoscale convective systems. *Preprints, Symp. on the Role of Clouds in Atmospheric Chemistry and Global Climate,* Amer. Meteor. Soc., 264–269.

Ninomiya, K., 1971: Dynamic analysis of outflow from tornado-producing thunderstorms as revealed by ATS III pictures. *J. Appl. Meteor.,* **10,** 275–294.

——, and T. Akiyama, 1974: Band structure of mesoscale echo associated with low-level jet stream. *J. Meteor. Soc. Japan,* **52,** 300–313.

Orlanski, I., 1975: A rational subdivision of scales for atmospheric processes. *Bull. Amer. Meteor. Soc.,* **56,** 527–530.

Palmen, E., and C. W. Newton, 1969: *Atmospheric Circulation Systems.* Academic Press, 603 pp.

Phillips, N. A., 1979: The nested grid model. NOAA Tech. Rep., NMC, 80 pp.

Rotunno, R., J. B. Klemp and M. L. Weisman, 1988: A theory for strong, long-lived squall line. *J. Atmos. Sci.,* **45,** 463–485.

Rutledge, S. A., and R. A. Houze, Jr., 1987: A diagnostic modeling study of the trailing stratiform region of a midlatitude squall line. *J. Atmos. Sci.,* **44,** 2640–2656.

——, ——, M. I. Biggerstaff and T. Matejka, 1988: The Oklahoma–Kansas mesoscale convective system of 10–11 June, 1985: Precipitation structure and single-Doppler radar analysis. *Mon. Wea. Rev.,* **116,** 1409–1430.

Sanders, F., and K. Emanuel, 1977: The momentum budget and temporal evolution of a mesoscale convective system. *J. Atmos. Sci.,* **34,** 136–330.

Schneider, E. K., and R. S. Lindzen, 1976: A discussion of the parameterization of momentum exchange by cumulus convection. *J. Geophys. Res.,* **81,** 3158–3160.

Smull, B. F., and R. A. Houze, Jr., 1985: A midlatitude squall line with a trailing region of stratiform rain: Radar and satellite observations. *Mon. Wea. Rev.,* **113,** 117–133.

——, and ——, 1987a: Dual-Doppler radar analysis of a midlatitude squall line with a trailing region of stratiform rain. *J. Atmos. Sci.,* **44,** 2128–2148.

——, and ——, 1987b: Rear inflow in squall lines with trailing stratiform precipitation. *Mon. Wea. Rev.,* **115,** 2869–2889.

Soong, S.-T., and W.-K. Tao, 1984: A numerical study of the vertical transport of momentum in a tropical rainband. *J. Atmos. Sci.,* **41,** 1049–1061.

Stevens, D. E., 1979: Vorticity, momentum and divergence budgets of synoptic-scale wave disturbance in the tropical Eastern Atlantic. *Mon. Wea. Rev.,* **107,** 535–550.

Thorpe, A. J., M. J. Miller and M. W. Moncrieff, 1982: Two-dimensional convection in non-constant shear: A model of midlatitude squall lines. *Quart. J. Roy. Meteor. Soc.,* **108,** 739–762.

Zhang, D.-L., 1989: The effect of parameterized ice microphysics on the simulation of vortex circulation with a mesoscale hydrostatic model. *Tellus,* **41A,** 132–147.

——, E.-Y. Hsie and M. W. Moncrieff, 1988: A comparison of explicit and implicit predictions of convective and stratiform precipitating weather systems with a meso-β scale numerical model. *Quart. J. Roy. Meteor. Soc.,* **114,** 31–60.

——, and J. M. Fritsch, 1987: Numerical simulation of the meso-β scale structure and evolution of the 1977 Johnstown flood. Part II: Inertially stable warm-core vortex and the mesoscale convective complex. *J. Atmos. Sci.,* **44,** 2593–2612.

——, and ——, 1988: Numerical sensitivity experiments of varying model physics on the structure, evolution and dynamics of two mesoscale convective systems. *J. Atmos. Sci.,* **45,** 261–293.

——, K. Gao and D. B. Parsons, 1989: Numerical simulation of an intense squall line during 10–11 June 1985 PRE-STORM. Part I: Model verification. *Mon. Wea. Rev.,* **117,** 960–994.

——, and ——, 1989: Numerical simulation of an intense squall line during 10–11 June 1985 PRE-STORM. Part II: Rear inflow, surface pressure perturbations and stratiform precipitation. *Mon. Wea. Rev.,* **117,** 2067–2094.

Zipser, E. J., R. J. Meitin and M. A. LeMone, 1981: Mesoscale motion field associated with a slowly moving GATE convective band. *J. Atmos. Sci.,* **38,** 1725–1750.